46th AIAA Aerospace Sciences Meeting and Exhibit
7 - 10 January 2008, Reno, Nevada

AIAA 2008-36

Performance of WENO Scheme in Generalized Curvilinear Coordinate Systems

Xiaodan Cai* and Foluso Ladeinde†
TTC Technologies, Inc., Suite 206B, 2100 Middle Country Road, Centereach, NY 11720

The weighted-essentially non-oscillatory (WENO) schemes have been used to calculate the shock-embedded compressible fluid flow ([9]). The potential high-fidelity qualities of this approach make it attractive for jet noise simulation. However, in its present form, the WENO procedure has many drawbacks that prevent direct applications to jet noise simulations. In this paper, various WENO procedures are evaluated in generalized curvilinear coordinate systems. In addition, freestream preservation and boundary treatment are discussed. It has been verified in this paper that the original WENO procedure drafted by Jiang and Shu ([9]) is too dissipative for shock/entropy wave interactions. It has also been found that the ghost-point boundary treatment suggested in [9] does not perform well for shock-boundary interaction problems and more general problems with solid walls. Furthermore, it is demonstrated that the modifications suggested by Martin et al. ([11], [12]) are susceptible to numerical oscillations in non-homogeneous compressible flows. A modified WENO scheme that is more robust and less dissipative is proposed and tested in this paper.

I. Introduction

Computational aeroacoustics (CAA) has made significant progress over the last decades, and offers new perspectives on jet noise understanding and predictions, as pointed out by Tam in 1998 ([1]). As the focus of current CAA computations of jet noise is on the development of high-fidelity large-eddy simulations (LES), various higher-order accurate and optimized numerical schemes are sought in order to reduce the required number of grid points per wavelength with low dissipation and low dispersion properties. The dispersion-relation-preserving (DRP) scheme has been used in the jet-noise predictions by Bogey and Bailly ([2]-[4]). The high-order compact scheme has been used in the work of Bodony and Lele ([5]), and Lyrintzis and co-workers ([6]). It has been noted that the above-mentioned high-order schemes are suitable only for subsonic jet flows. For supersonic jet flow with shock-associated noises, very few work, except those of Shur et al ([7], [8]) that have been attempted with high-order numerical schemes.

In the work of Shur et al. ([7], [8]), a high-order hybrid scheme (weighted 5^{th}-order upwind and 4^{th}-order centered MUSCL scheme) are used. As the weighted-essentially non-oscillatory (WENO) methods are developed to tackle the shock-embedded compressible fluid flow ([9]), the WENO scheme shows a potential in simulating supersonic jet noises ([10]). However, it has been noticed that the original WENO scheme developed in ([9]) is too dissipative, and it can be improved by the procedure developed in Martin et al ([10], [11]) for homogeneous flows. As the improvement by Martin et al. is based on the numerical analysis with uniform grids and ignores the issues related to the WENO treatment of boundary conditions, the current study provides a further evaluation of the performance of Martin's scheme in more complex flows with general curvilinear systems. Some issues arising from the WENO treatment of boundary conditions are also addressed in this paper.

The WENO scheme developed in the current work is based on a finite difference procedure for the convective flux terms as proposed by Jiang and Shu ([9]). One of the principal problems encountered in the solution of the Navier–Stokes equations with high-order finite-difference schemes in general curvilinear coordinates is the occurrence of numerical instabilities which are very sensitive to the nonlinear interactions from boundary condition implementation, mesh non-uniformities, unresolved flow scales, and the nonlinearity of the governing equations.

* Senior Research Engineer, AIAA Member.
† Director of Research, AIAA Associate Fellow.

The mesh non-uniformities cause an issue of freestream preservation and metric cancellations. These errors, which arise in finite-difference discretizations of the governing equations written in strong-conservation form, can catastrophically degrade the fidelity of higher-order approaches, which have been addressed carefully for high-order compact schemes by Visbal and Gaitonde ([13]). However, for the WENO scheme, since the metrics need to be evaluated in an adaptive, weighted mode as the flux terms were, the exact metric cancellation is difficult to achieve. Thus the overall WENO performance turns out being dependent somewhat on the mesh qualities (Cai et al. (2000)). A numerical procedure has been developed in this paper to handle this issue. Meanwhile, it is worthy to note that an alternative WENO implementation based on the Roe approximate Riemann solver has also appeared in the literature (for example, Gross and Fasel, 2002; Shen, Wang and Zha, 2007). In this approach, the WENO procedure is used to reconstruct the primitive/conservative variables at the cell faces, and plays a role as the limiter. Therefore, the procedure for the metrics calculations for the conventional Roe schemes can then be extended straightforward to the WENO calculations, and the issues of freestream preservations and metric cancellations can be treated as usual. The performance of this WENO procedure in general curvilinear coordinate systems is currently under investigation in our organization, and will be reported in our future reports.

The paper is organized as follows. In Section II, the basic WENO form in a general curvilinear coordinate system is given. The issues on the freestream preservation and boundary treatments are then discussed in Sections III and IV. Section V presents the numerical experiments of various WENO schemes on a series of test cases with different complexities from solid-wall boundaries and non-uniform mesh systems. A summary of our observations has been drawn in Section VI.

II. WENO Procedure in a Curvilinear Coordinate System

Our WENO scheme is implemented for a flow in a curvilinear coordinate system, which is in the form

$$\frac{\partial (Q/J)}{\partial t}+\frac{\partial \hat{F}}{\partial \xi}+\frac{\partial \hat{G}}{\partial \eta}+\frac{\partial \hat{H}}{\partial \zeta}=\frac{\partial \hat{F}_v}{\partial \xi}+\frac{\partial \hat{G}_v}{\partial \eta}+\frac{\partial \hat{H}_v}{\partial \zeta}, \tag{1}$$

where Q is the vector of conserved variables, $Q=(\rho,\rho u,\rho v,\rho w,\rho E)^T$, $(\hat{F},\hat{G},\hat{H})$ are the convective fluxes, $(\hat{F}_V,\hat{G}_V,\hat{H}_V)$ are the viscous fluxes, J is the Jacobian of the transformation between the generalized coordinate system (ξ,η,ζ), and physical coordinate system (x, y ,z). The WENO scheme is used to approximate the convective flux terms with Roe-type characteristic decomposition, i.e.,

$$\left.\frac{\partial \hat{F}}{\partial \xi}\right|_i=\frac{1}{\Delta \xi}\left\{\left[\tilde{R}_{Roe}\cdot\left(\tilde{R}_{Roe}^{-1}\cdot\hat{F}\right)\right]_{i+1/2}-\left[\tilde{R}_{Roe}\cdot\left(\tilde{R}_{Roe}^{-1}\cdot\hat{F}\right)\right]_{i-1/2},\right\}, \tag{2}$$

where $\tilde{R}_{Roe}$ is the matrix formed with the right eigenvectors of the Jacobian $\partial\hat{F}/\partial Q$ computed based on a Roe-averaged state at $i\pm½$. For the characteristic WENO, the reconstruction procedure is performed on the characteristic fields $\hat{F}_c=\tilde{R}_{Roe}^{-1}\cdot\hat{F}$ to obtain the values at $i+½$, which are

$$\begin{aligned}\hat{F}^{-}_{c,i+1/2}&=\sum_{r=0}^{k-1}\omega_r F^{(r)-}_{c,i+1/2},\\ F^{(r)-}_{c,i+1/2}&=\sum_{m=0}^{k-1}c_{rm}\hat{F}_{c,i-k+r+m+1},\end{aligned} \tag{3}$$

where $\hat{F}^{\pm}_{c,i+1/2}$ are the WENO reconstructed values of $\hat{F}_{c,i+1/2}$ from the left- and right-sides, respectively. k indicates the number of candidate stencils, which is fixed to 3 in the current study. ω_r are the normalized forms of weights, Ω_r, which are based on smoothness indicators, IS_r, of the numerical fluxes,

$$\Omega_r=\frac{C_r}{(\varepsilon+IS_r)^p}, \tag{4}$$

in which ε prevents division by zero, and p may be varied to increase or decrease WENO adaptation sensitivity. Both parameters are found to affect the WENO dissipations, where the smaller value of ε or the larger value of p induces the more dissipation of the WENO schemes. $\varepsilon=10^{-6}$ and $p=2$ are suggested in the work of Jiang and Shu ([9]), while $\varepsilon=10^{-10}$ and $p=1$ are adopted in Martin et al. ([10], [11]). IS_r is a smoothness measurement that becomes large when discontinuities are present within stencil r. In Martin et al. ([10], [11]), the concept of limiters is proposed to gauge the value of IS_r so that often adaptations of the WENO stencils are restricted. The weighing constants, C_r for both WENO schemes are listed in Table 1 for $k=3$, where the scheme by Jiang and Shu is noted as WENO-JS, and the scheme by Martin et al. as WENO-PM. WENO-PM (SYMOO) and WENO-PM (SYMBO) are two variants of WENO-PM. When there is no explicit identification, WENO-PM is always referred to WENO-PM (SYMBO) with the total variation relative limiters (RLTV). c_{rm} represents the coefficients of Lagrange interpolation, which are the same for both WENO-JS and WENO-PM and are listed in Table 2. It is also noted that the number of candidate stencils are different in the two schemes, in which a symmetric WENO stencil ($k=4$) are proposed in the work of Martin et al. The determination of the smoothness indicators (IS_r) from various WENO schemes is described as follows:

- **Smoothness Indicator**

The basic formula for the smoothness indicator is

$$IS_r = \sum_{m=1}^{k-1}\left(\sum_{l=0}^{k-1} d_{rml}^{k} F_{i-k+r+l+1}\right)^2, \tag{5}$$

where the coefficients are listed in Table 3.

WENO-JS regulates IS_r by using the limiter

$$IS_r = \begin{cases} 0, & IS_k < \alpha_{AL} \\ IS_r, & otherwise \end{cases} \tag{6}$$

where α_{AL} is a case-dependent, empirical constant. In our calculations, α_{AL} is set to zero as in Jiang and Shu (1996).

WENO-PM (RL) uses the limiter

$$IS_r = \begin{cases} 0, & R(IS) < \alpha_{RL} \\ IS_r, & otherwise \end{cases} \tag{7}$$

where

$$R(IS) = \frac{\max_{0\le r\le k} IS_r}{\varepsilon + \min_{0\le r\le k} IS_r},$$

and α_{RL} is taken as 10.

WENO-PM (RLTV) is using the limiter

$$IS_r = \begin{cases} 0, & R(TV) < \alpha_{RL}^{TV} \\ IS_r, & otherwise \end{cases} \tag{8}$$

in which

$$R(TV) = \frac{\max_{0\le r\le k} TV_r}{\varepsilon + \min_{0\le r\le k} TV_r},$$

$$TV_r = \sum_{l=1}^{k-1} \left| F_{i-k+r+l+1} - F_{i-k+r+l} \right|,$$

and $\alpha_{RL}^{TV} = 5.0$.

r	**WENO-JS**	**WENO-PM** (SYMOO)	**WENO-PM** (SYMBO)
0	1/10	1/20	0.094647545896
1	6/10	9/20	0.428074212384
2	3/10	9/20	0.408289331408
3	N/A	1/20	0.068988910311

Table 1: Optimal weights C_r with *k=3*

c_{rm}	**m=0**	**m=1**	**m=2**
r=0	2/6	-7/6	11/6
r=1	-1/6	5/6	2/6
r=2	2/6	5/6	-1/6
r=3 (WENO-PM only)	11/6	-7/6	2/6

Table 2: Candidate flux stencil coefficients c_{rm} for both WENO-JS and WENO-PM

d_{rml}		***l=0***	***l=1***	***l=2***
m=1	*r=0*	1/2	-4/2	3/2
	r=1	-1/2	0	1/2
	r=2	-3/2	4/2	-1/2
	r=3	-5/2	8/2	-3/2
m=2	*r=0*	β_2	-2 β_2	β_2
	r=1	β_2	-2 β_2	β_2
	r=2	β_2	-2 β_2	β_2
	r=3	β_2	-2 β_2	β_2

Table 3: Smoothness measurement stencil coefficients d_{rml} for both WENO-JS and WENO-PM. Note *r=3* is relevant only for WENO-PM.

III. Freestream Preservation and Metric Cancellation

Freestream preservation and metric cancellation issues arise when high-order numerical schemes are used to discretize Eq. (1). Thus the metric identities (I_ξ,I_η, and I_ζ), for example,

$$I_\xi = \left(\frac{\xi_x}{J}\right)_\xi + \left(\frac{\eta_x}{J}\right)_\eta + \left(\frac{\zeta_x}{J}\right)_\zeta = 0, \qquad (9)$$

must be satisfied by various numerical discretizations.

A direct evaluation of the metrics,

$$\begin{aligned} \xi_x / J &= y_\eta z_\zeta - y_\zeta z_\eta, \\ \eta_x / J &= y_\zeta z_\xi - y_\xi z_\zeta, \\ \zeta_x / J &= y_\xi z_\eta - y_\eta z_\xi. \end{aligned} \qquad (10a)$$

is working well for high-order numerical schemes as pointed out by Visbal and Gaitonde ([13]). For the compact scheme described in that paper, Visbal and Gaitonde have designed a conserving procedure to evaluate the metrics,

$$\begin{aligned}\xi_x / J &= (y_\eta z)_\zeta - (y_\zeta z)_\eta,\\ \eta_x / J &= (y_\zeta z)_\xi - (y_\xi z)_\zeta,\\ \zeta_x / J &= (y_\xi z)_\eta - (y_\eta z)_\xi.\end{aligned} \tag{10b}$$

These metric forms are adopted in our WENO implementations. Furthermore, considering that the WENO scheme is an upwind-weighted scheme, the metric evaluation of any first-derivative appearing in Eq. (10b) is treated by an averaging procedure as follows, taking x_ξ as an example:

$$\begin{aligned}\left(x_\xi\right)_i &= \left(\hat{x}_{i+1/2} - \hat{x}_{i-1/2}\right),\\ \hat{x}_{i+1/2} &= \frac{1}{2}(x^+_{i+1/2} + x^-_{i+1/2}),\end{aligned} \tag{11}$$

where $x^+_{i+1/2}$ and $x^-_{i+1/2}$ are evaluated by a WENO procedure as above, respectively, interpolated from the left and right hand sides. Our experience shows, use of Eq. (11) reduces the numerical errors in evaluating Eq. (9) by two orders of magnitude. Table 4 gives the numerical errors from various numerical schemes in evaluating the metrics and the identity using Eq. (9) for a typical 2D curvilinear mesh of airfoil.

Scheme	$\varepsilon(\xi_x)$	$\varepsilon(\eta_x)$	$\varepsilon(\eta_y)$	$\varepsilon(\mathrm{I}_\xi)$
2nd-Central Difference	1.58×10^{-5}	2.22×10^{-2}	5.11×10^{-5}	4.62×10^{-18}
6th-Compact	2.76×10^{-8}	6.08×10^{-4}	1.35×10^{-8}	3.93×10^{-17}
5th-WENO	3.63×10^{-6}	8.44×10^{-3}	2.65×10^{-6}	2.39×10^{-7}

Table 4: Numerical Errors from various schemes in evaluating metric identity I_ξ

To further reduce the numerical effects of the metrics evaluation errors, the full form of Navier-Stokes equation in the curvilinear coordinate systems,

$$\frac{\partial(Q/J)}{\partial t} + \frac{\partial \hat{F}}{\partial \xi} + \frac{\partial \hat{G}}{\partial \eta} + \frac{\partial \hat{H}}{\partial \zeta} - \frac{\partial \hat{F}_v}{\partial \xi} + \frac{\partial \hat{G}_v}{\partial \eta} + \frac{\partial \hat{H}_v}{\partial \zeta} = -(F + F_v)\cdot I_\xi - (G + G_v)\cdot I_\eta - (H + H_v)\cdot I_\zeta, \tag{12}$$

is used in place of Eq. (1).

IV. Boundary Treatment

It is noted that in Shu (1997), ghost points with artificially-set large values are used to evaluate the flux terms at the boundaries This procedure, which is equivalent in force to the use of a one-sided stencil, induces significant numerical errors as demonstrated later in this work. Our remedy is to design a lower order (second-order) fixed stencil to approximate the flux terms $\hat{F}_{1/2}$ and $\hat{F}_{N-1/2}$ near the boundaries, and lower WENO schemes for the next near-boundary points. Specifically, under this new treatment, the equations in Eq. (3) are reformulated below.

a) WENO Evaluation of Flux Terms at Boundaries

For the first half points, we have

$$\begin{aligned}\hat{F}_{c,i\,1/2} &= \frac{1}{2}\left(\hat{F}_0 + \hat{F}_1\right),\\ \hat{F}_{c,iN-1/2} &= \frac{1}{2}\left(\hat{F}_{N-1} + \hat{F}_N\right).\end{aligned} \tag{13}$$

For the second close-boundary cell-face points, a WENO procedure with k=2 are used. The schemes with these modifications are called MWENO. It is noted that ε=10^{-10} and p=1 are adopted for MWENO in our calculations, as the modified schemes by Martin et al.

A WENO-consistent one-sided interpolation procedure has also been derived for the boundary conditions with the gradients specified. The formulas are described below.

b) WENO Interpolation of *dφ/dn* at Boundaries

It is known from the WENO procedure reported by Shu in 1997 that the interpolation function and its derivative from the cell-averaged values of $\overline{\varphi}$, are

$$\varphi(x)=\sum_{j=0}^{k-1}\left(\sum_{m=j+1}^{k}\frac{\sum_{l=0,l\neq m}^{k}\prod_{q=0,q\neq m,l}^{k}\left(x-x_{i-r+q-1/2}\right)}{\prod_{l=0,l\neq m}^{k}\left(x_{i-r+m-1/2}-x_{i-r+l-1/2}\right)}\right)\Delta x_{i-r+j}\overline{\varphi}_{i-r+j}, \tag{14a}$$

$$\varphi'(x)=\sum_{j=0}^{k-1}\left(\sum_{m=j+1}^{k}\frac{\sum_{l=0,l\neq m}^{k}\sum_{q=0,q\neq m,l}^{k}\prod_{n=0,n\neq m,l,q}^{k}\left(x-x_{i-r+q-1/2}\right)}{\prod_{l=0,l\neq m}^{k}\left(x_{i-r+m-1/2}-x_{i-r+l-1/2}\right)}\right)\Delta x_{i-r+j}\overline{\varphi}_{i-r+j}. \tag{14b}$$

Therefore, we have at the cell-center point,

$$\varphi_i=\varphi(x_i)=\sum_{j=0}^{k-1}\left(\sum_{m=j+1}^{k}\frac{\sum_{l=0,l\neq m}^{k}\prod_{q=0,q\neq m,l}^{k}\left(x_i-x_{i-r+q-1/2}\right)}{\prod_{l=0,l\neq m}^{k}\left(x_{i-r+m-1/2}-x_{i-r+l-1/2}\right)}\right)\Delta x_{i-r+j}\overline{\varphi}_{i-r+j}, \tag{15a}$$

$$\left.\frac{d\varphi}{dx}\right|_{x_i}=\varphi'(x_i)=\sum_{j=0}^{k-1}\left(\sum_{m=j+1}^{k}\frac{\sum_{l=0,l\neq m}^{k}\sum_{q=0,q\neq m,l}^{k}\prod_{n=0,n\neq m,l,q}^{k}\left(x_i-x_{i-r+n-1/2}\right)}{\prod_{l=0,l\neq m}^{k}\left(x_{i-r+m-1/2}-x_{i-r+l-1/2}\right)}\right)\Delta x_{i-r+j}\overline{\varphi}_{i-r+j}. \tag{15b}$$

For k=3, r=-1, and a uniform grid, we have

$$\varphi_i=\frac{23}{24}\overline{\varphi}_i+\frac{1}{12}\overline{\varphi}_{i+1}-\frac{1}{24}\overline{\varphi}_{i+2}, \tag{16a}$$

$$\frac{d\varphi_i}{dx}=\frac{1}{2}\left(-3\overline{\varphi}_i+4\overline{\varphi}_{i+1}-\overline{\varphi}_{i+2}\right). \tag{16b}$$

Equations (16a) and (16b) can be used to approximate the boundary values as the gradient at the boundary is known. For example, with $d\varphi/dn = 0$, we can extrapolate from the interior points, the boundary values as

$$\varphi_i = \frac{49}{36}\overline{\varphi}_{i+1} - \frac{13}{36}\overline{\varphi}_{i+2} \quad . \tag{17}$$

V. Numerical Results

a) Free Stream on a Curvilinear Mesh

A uniform free-stream flow with a Mach number of 1 is imposed on a curvilinear mesh as used in Visbal and Gaitonde ([19]). The mesh is uniform in the x-direction, but is stretched in the y-direction as specified by

$$\begin{aligned} x_{i,j} &= x_{\min} + \Delta x \cdot (i-1) \\ y_{i,j} &= \left(y_{\min} + \Delta y \cdot (j-1)\right) + A \cdot \sin\left(R \cdot \pi \cdot x + j \cdot \phi / JL\right) \end{aligned} \tag{18}$$

The grid quality is dependent on the choice of the parameter of A, R, and Φ. In our test, $\Delta x = 0.1$, $R = 16$, $\phi = 3/2 \cdot \pi$ and $A = 0.1 \cdot \exp(-0.1 \cdot \left({x_{i,j}}^2 + {y_{i,j}^0}^2 \right))$ where $y_{i,j}^0 = y_{\min} + \Delta y \cdot (j-1)$. The choice of the parameter A is determined by a way so that the stretched mesh is located away from the boundary (as shown in Figure 1a). If the metrics cancellation is not carefully treated, significant numerical oscillation occurs as seen in Figure 1b. After Eqs (11) and (12) have been used, no visible pressure oscillations have been observed.

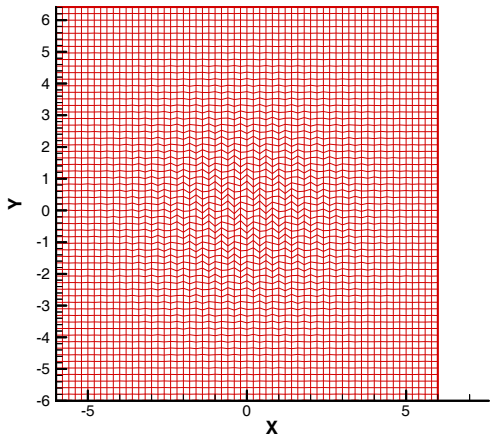

Figure 1a: Curvilinear mesh with stretched grid away from the boundary.

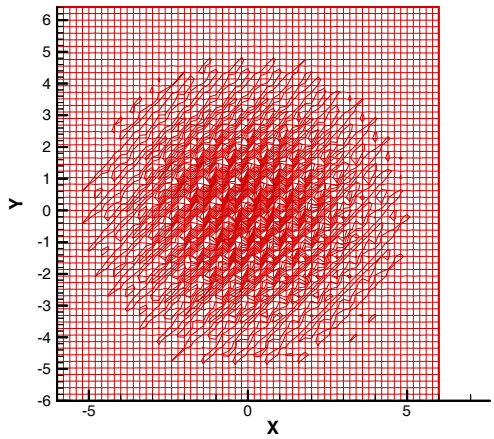

Figure 1b: Pressure contour distributions for a uniform free-stream flow calculated with WENO scheme without exact metrics cancellations.

b) 1D Shock-Wave Interaction

This test problem includes the propagation of a moving shock interacting with a density fluctuation. The parameters chosen in the current study are exactly consistent with those in Taylor et al. ([11]), which provide a validation case for the implementation of WENO-PM scheme. The initial condition is specified as

$$\left[\rho, \quad u, \quad p\right] = \begin{cases} \left[3.857143, \quad 2.629369, \quad 10.333333\right], & x < 0.125 \\ \left[1 + 0.2\sin(16\pi \cdot x), \quad 0, \quad 1\right], & x \geq 0.125 \end{cases} \tag{19}$$

The domain size is [0.0, 1.0] with 192 grid points distributed uniformly as the same as in [11].

Figures 2a and 2b present the density profiles from various WENO schemes, compared to exact solutions and MUSCL-Roe scheme. It is shown that the original WENO-JS is indeed very dissipative and only slightly better than the MUSCL-Roe scheme. On the other hand, the MWENO scheme with $\varepsilon=10^{-10}$ and $p=1$ improves the results significantly, and the WENO-PM scheme compares excellent with the exact solution as well as those in [11].

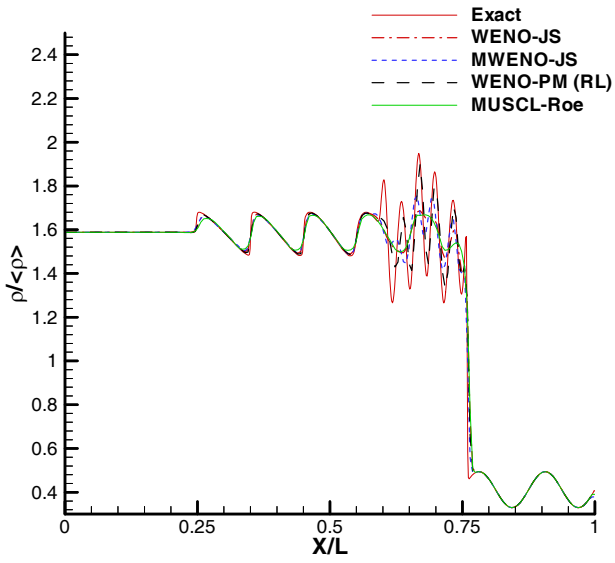

Figure 2a: Density profiles from various WENO schemes.

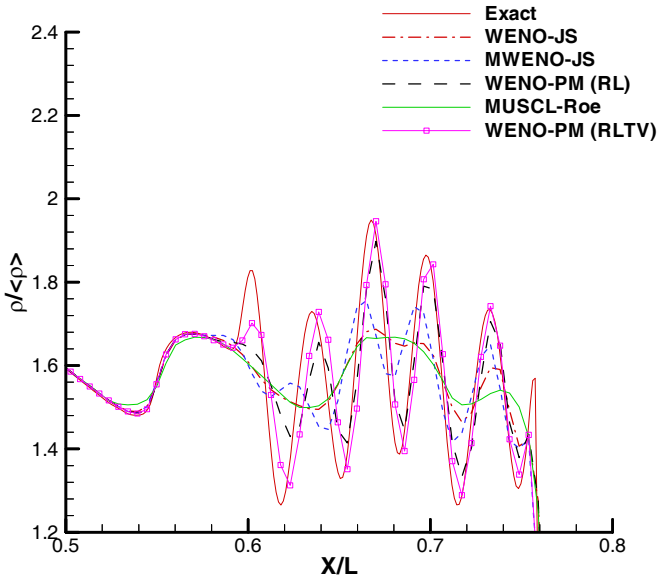

Figure 2b: Comparison of schemes in fluctuation regions. Note that WENO-PM (RLTV) is shown here and MUSCL-Roe is not shown here.

c) Inviscid Oblique Shock Interaction

This is a two-dimensional test case. The freestream Mach number and flow deflection angle are $M_\infty=3.0$ and $\delta=15^\circ$, respectively, as used in Visbal and Gaitonde ([12]). The mesh size is 151×51 and is uniformly distributed in both directions.

Figure 3 presents the pressure distributions along the line *y=0.1*. The results show that the original WENO-JS with large-valued ghost points induces significant oscillations and wrong reflective shock-wave positions. Meanwhile, when symmetric boundary conditions are used, the WENO-JS produces a profile in much better agreement with the exact solution, which demonstrates that the boundary treatments indeed affect the performance of the WENO scheme. Considering the complexity in implementing the symmetric boundary conditions for general geometric-complex cases, it is our choice to use the MWENO-JS scheme with first-order extrapolation and MWENO-JS2 with second-order WENO-consistent extrapolation in Eq. (20). Figure 3a shows that both WENO-JS and WENO-JS2 perform well. Furthermore, Figure 3b shows that the MWENO-JS performs much better that MUSCL-Roe scheme while the WENO-PM scheme induces significant oscillations. Figure 4(a) presents the pressure contours from MWENO-JS which is oscillation-free, compared with the oscillatory results from WENO-PM in Figure 4(b). The uniform-distributed meshes are also shown in Figure 4(a).

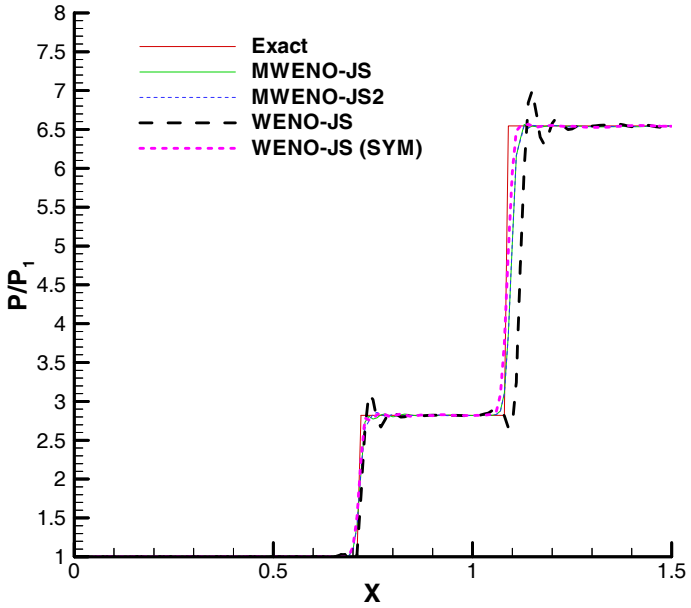

Figure 3a: Pressure distributions along *y=0.1* for Mach 3 inviscid shock reflection with different boundary schemes.

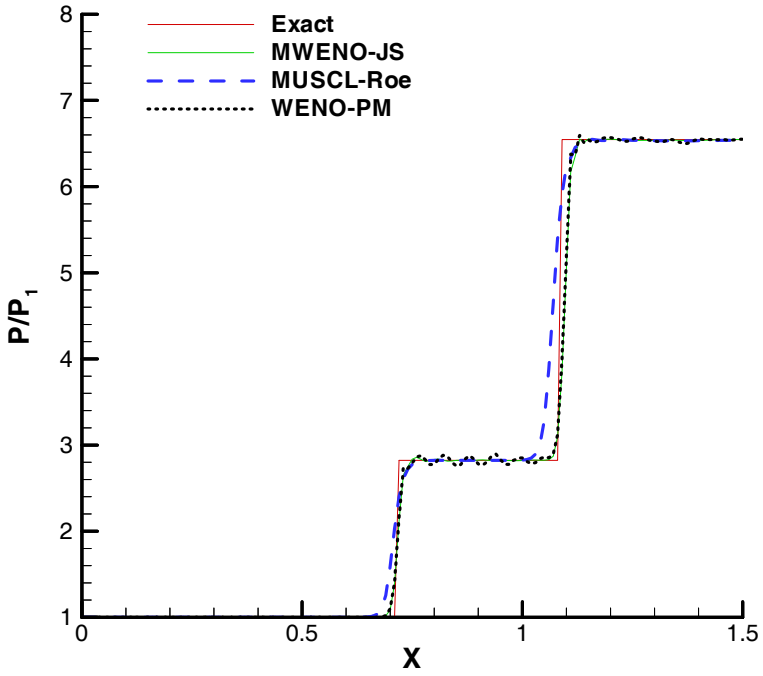

Figure 3b: Pressure distributions along *y=0.1* for Mach 3 inviscid shock reflection with different schemes.

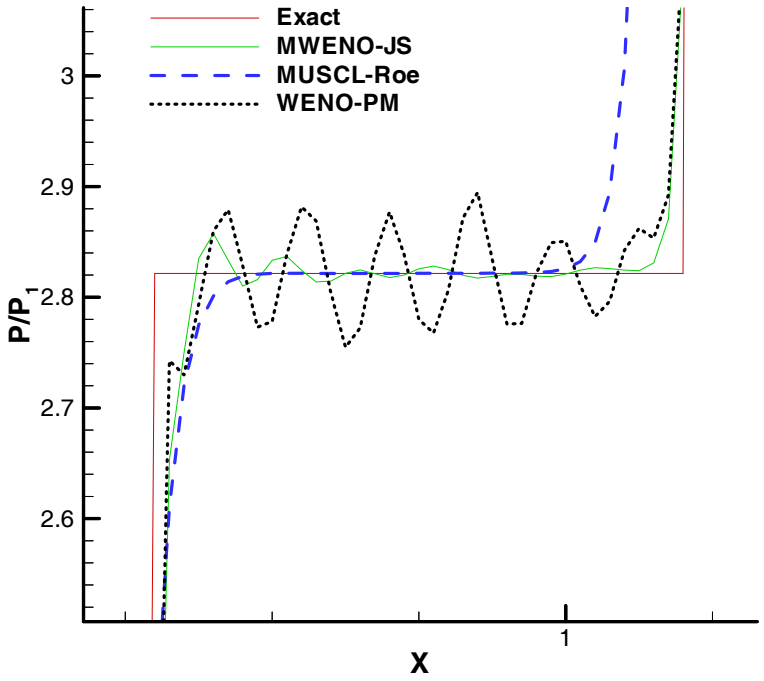

Figure 3c: A close-up view of pressure distributions along *y=0.1*.

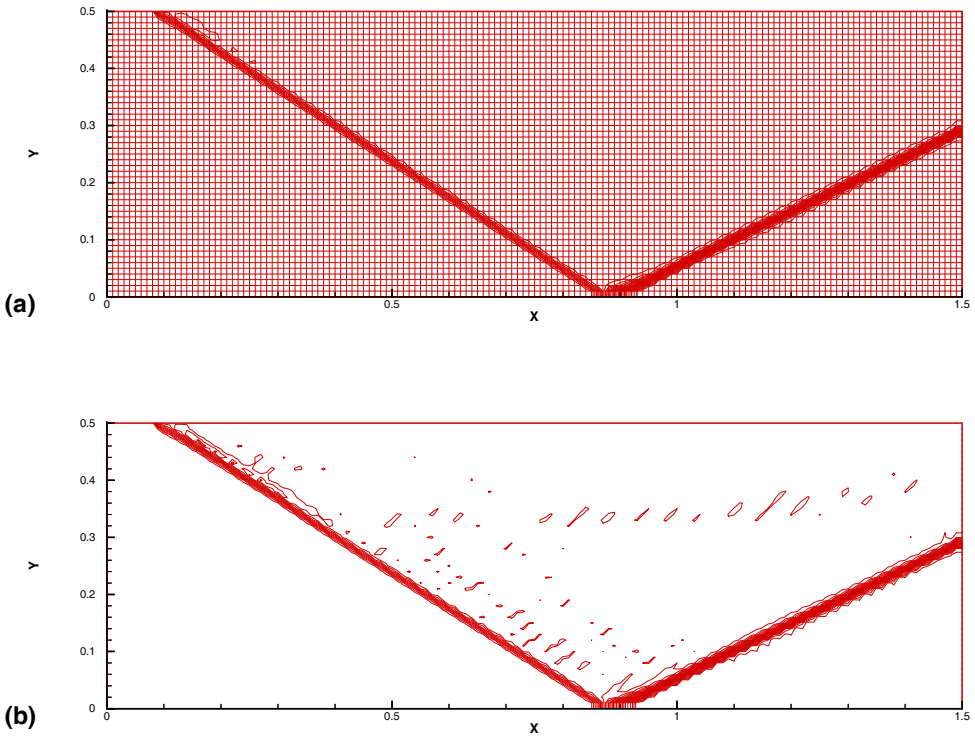

Figure 4: Pressure contours: (a) MWENO-JS; (b) WENO-PM.

d) 2D Shock/Laminar Boundary Layer Interaction

In this example, a complex separated flow is generated from the impingement of an oblique shock on a laminar boundary layer along a flat plate (see Visbal (2005)). The freestream Mach number is of 2.0 with 6° shock deflection angle. The Reynolds number is 3.0×10^5. The boundary setup and mesh used are the same as in Visbal (2005). That is, at the inflow boundary, fixed-flow boundary conditions obtained from a separate flat-plate computation are specified. Along the wall, no-slip adiabatic conditions are prescribed. At the top and outflow boundaries, first order extrapolation condition of all flow variables is used.

Figures 5 and 6 show the computational results with the grid size (286×131), the coarsest grid used in Visbal (2005). Compared with MUSCL-Roe scheme (Figure 5b), the MWENO-JS scheme (Figure 5a) produces a better compression/expansion waves above the separation zones. The surface pressure distributions shown in Figure 6a demonstrate that the MWENO-JS scheme produces much better results than the MUSCL-Roe scheme both upstream and downstream of the separation point, but does not improve the prediction on the location of the separation point. Meanwhile, the WENO-PM scheme produces an oscillatory surface pressure distribution. Figure 5c presents the pressure contours for WENO-PM. For comparison, Figure 5d show the results from a fine mesh (476×265). Figure 6b shows the results from MWENO-JS scheme converged to Visbal's fine-mesh results when the mesh is refined. The slight difference between the fine-mesh results could come from the fact that our simulation may not be fully converged.

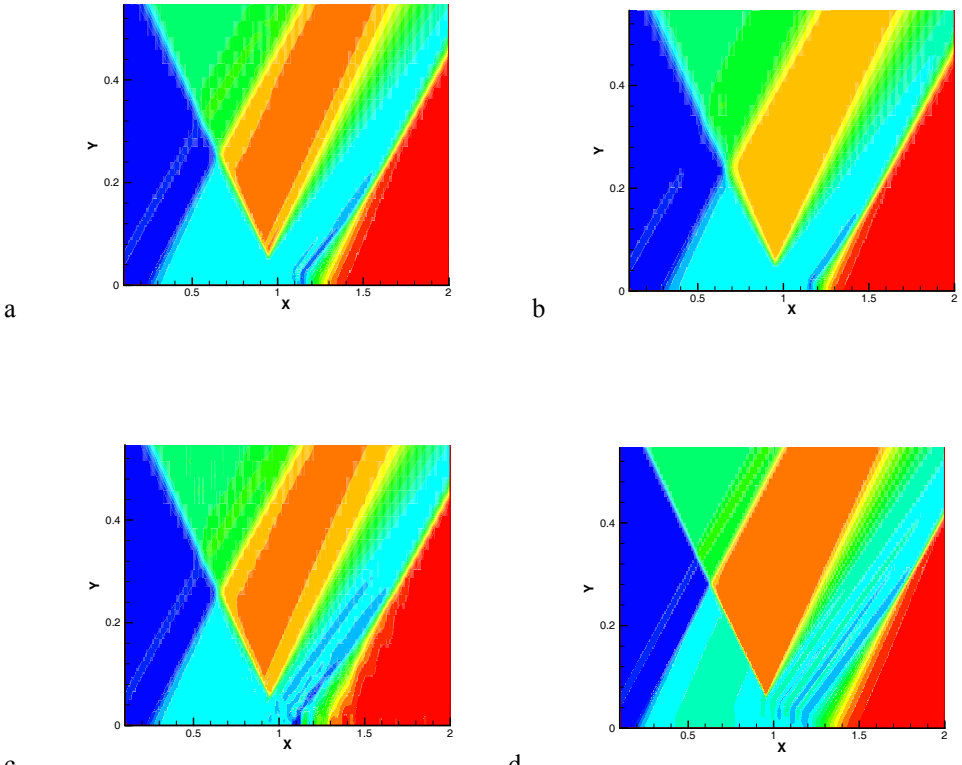

Figure 5: Pressure contours in shock/boundary layer interaction region: a) MWENO-JS; b) MUSCL-Roe; c) WENO-PM; d) MWENO (Fine mesh).

a

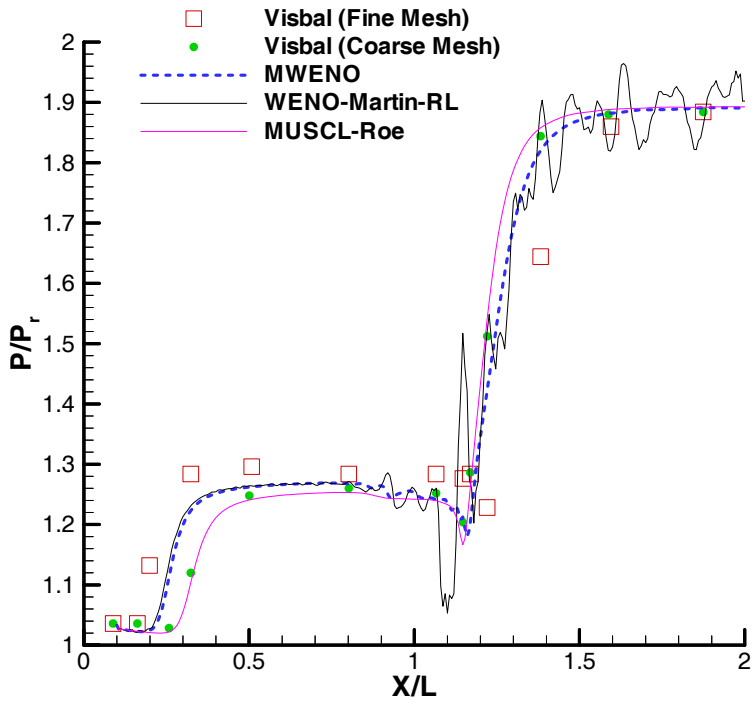

b

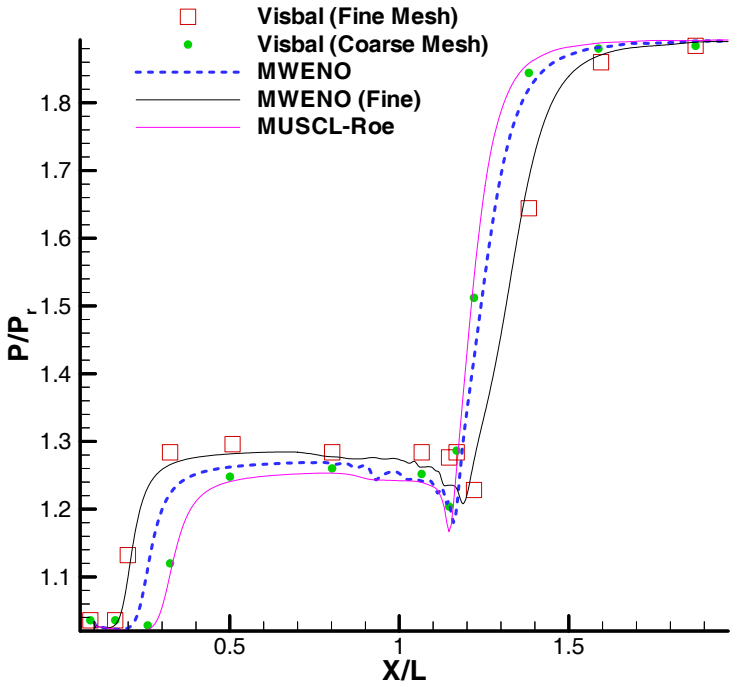

Figure 6: Surface pressure for Mach 2 shock/laminar boundary-layer interaction: a) MWENO compared with WENO-PM; b) Fine mesh versus coarse mesh.

e) Transonic Airfoil

In this example, a transonic flow around a NACA0012 airfoil has been simulated with O-grids (the mesh size is 193×40, as shown in Figure 7a). The computational domain size is 25, the Mach number is 0.8, and the angle of attach is 1.25. This is an inviscid calculation with slippery-wall boundary condition used at the airfoil surface. At the far field, the following Dirichlet boundary conditions are used without the vortex correction introduced by Thomas and Salas ([16]),

$$u = U_\infty \cos(\alpha), \quad v = U_\infty \sin(\alpha), \quad p = P_\infty, \quad \rho = \rho_\infty \ .$$

The typical pressure contours from the MWENO-JS are shown in Figure 7b. Figure 8 compares the convergence rate of the lift coefficients from various schemes, which show that the MWENO-JS has a slower convergence rate than the MUSCL-Roe scheme, but with a better convergence value than the MUSCL-Roe scheme. The original WENO-JS scheme can only obtain a quasi-steady solution. It is also noted that Jameson's result was obtained from a finer mesh with the mesh size of 320×64. Figure 9 compares the pressure coefficients around the top and bottom surfaces of the airfoil, which show that the results from the MWENO-JS scheme agree the best with Jameson's results.

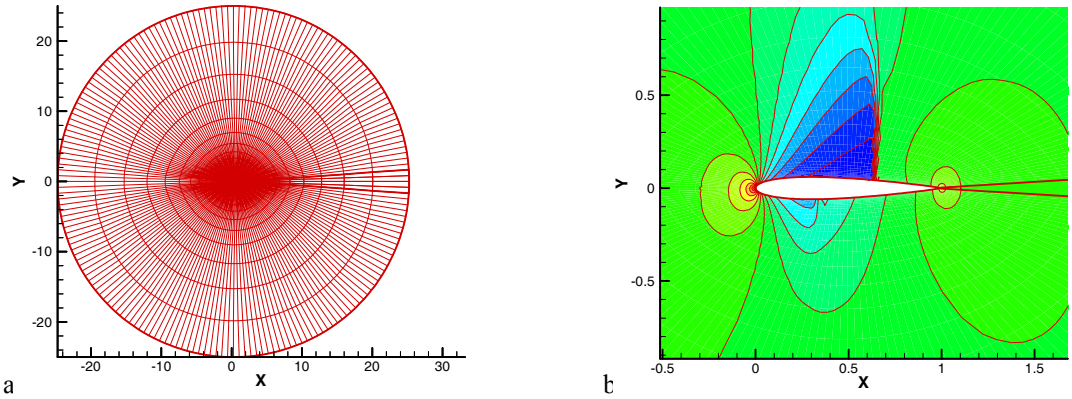

Figure 7: Transonic NACA0012 calculation: a) O-Mesh; b) Pressure contours from MWENO-JS.

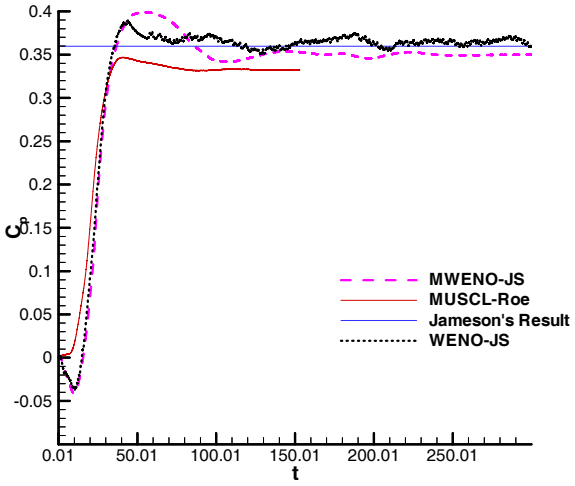

Figure 8: The convergence history of lift coefficients for various numerical schemes compared with the target converged solution of Jameson ([15]).

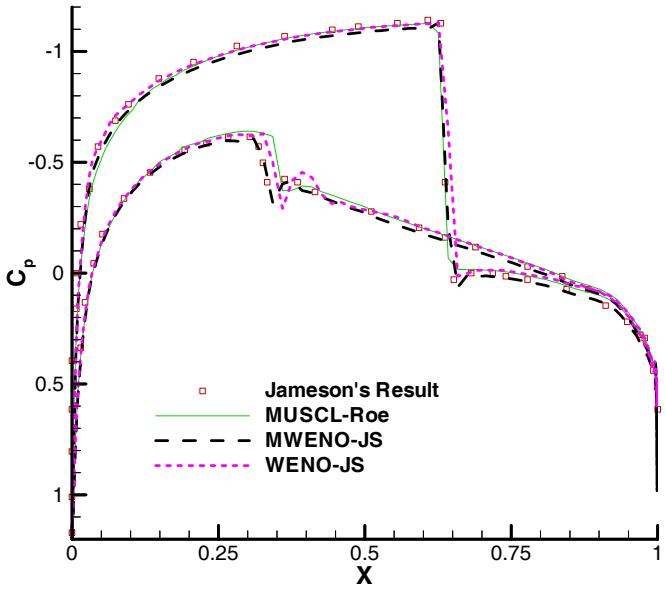

Figure 9: The surface pressure coefficients around the top and bottom surfaces of NACA0012 airfoil. M=0.8, α=1.25º.

f) High Subsonic Jet Flow

In this test, a high subsonic jet flows (M_j=0.9), the set point 7 of Tanna ([20]) is used to evaluate the performance of the modified WENO scheme. In a series of prior work by the authors (for example, Cai et al. ([21])), we have developed a hybrid LES/RANS numerical procedure, which successfully predicted the near-field SPL signatures and the far-field sound directivity pattern for a set of high subsonic jet flows. However, we also found that our hybrid LES/RANS procedure based on the MUSCL-Roe scheme has systematically over-predicted the near-field and far-field sound level by 5-10 dB, which is fortuitously consistent with many other works in the literature but need further investigations. It thus motivates us to apply the WENO scheme modified here for this case.

A multi-block mesh system with about two million grid points has been used in our calculations. The details about the mesh distributions, the far-field boundary treatment and the nozzle inflow conditions can be found in Cai et al. ([21]). The effects of the numerical schemes have been shown in Figure 10 through Figure 12. Figure 10 shows the averaged axial velocity at the jet centerline for three numerical schemes (MUSCL-Roe, WENO, and compact scheme). The results from the compact scheme are obtained from Bodony and Lele ([5]). It can be seen from Figure 10 that the numerical prediction from the WENO scheme compares well with the compact scheme, both of which are slightly better than that from the MUSCL-Roe scheme. The near-field pressure spectra at two locations (x/D=0.375, r/D=0.875; x/D=4.125, r/D=1.625) are shown in Figure 11. For the near-nozzle locations (for example, x/D=0.375), the numerical results with the WENO scheme appear to capture the distinctive tones occurred in the experimental data, which is not observed with MUSCL scheme. For down-stream locations (x/D=4.125), the LES with WENO scheme lowered the peak pressure level by about 10 dB than that with MUSCL scheme, which are closer to the experimental measurements. The numerical prediction on the far-field OASPL is shown in Figure 12, which is obtained from the near-field LES results by the Ffowcs-Williams/Hawkings (FW-H) integration method. The details about the validation and accuracy of our FW-H method can be found in Cai et al. ([21]). Figure 12 presents the sound directivities predicted by the WENO and MUSCL schemes (r/D=100), and also shows the effects by the locations of the FW-H integration surfaces (W_i denotes various span-wise widths and L_i for downstream locations, which is defined in Cai et al. ([21]). Once again, it confirms that the WENO scheme as well as the compact scheme performs better than the MUSCL scheme.

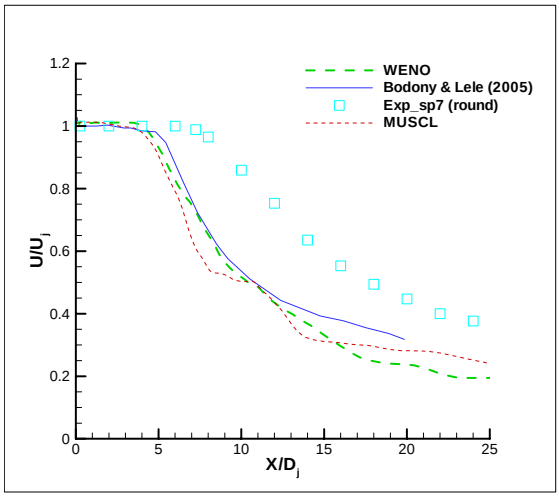

Figure 10: Centerline Mean Streamwise Velocity Profile.

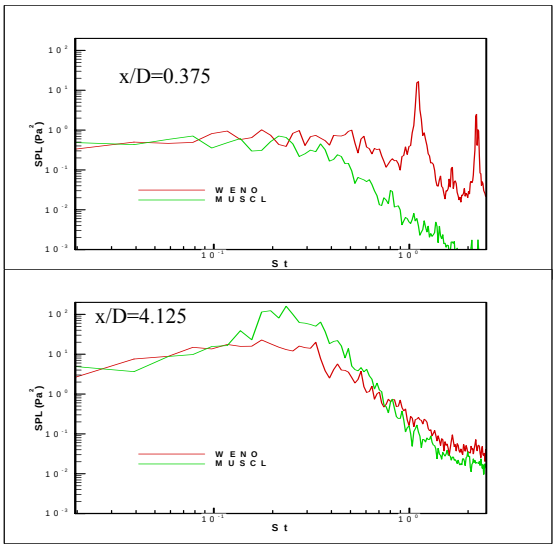

Figure 11: The near-field pressure spectra at two downstream locations predicted by the WENO and MUSCL Schemes.

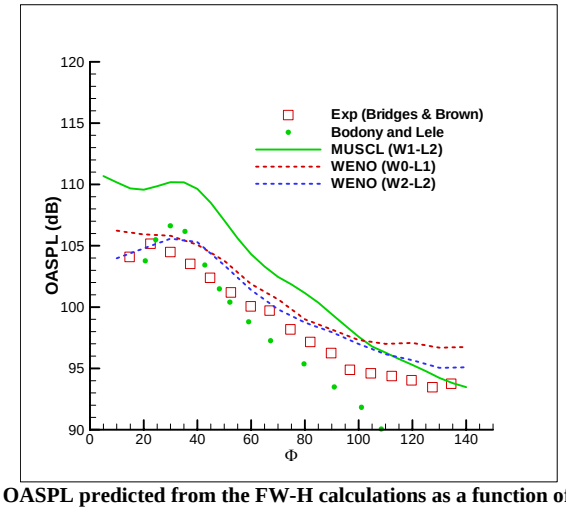

Figure 12: The OASPL predicted from the FW-H calculations as a function of the directivity angle.

VI. Summary and Future Work

In this paper, the original WENO procedure by Shu ([9]) has been modified to applications in generalized curvilinear coordinate systems. The issues on freestream preservation and boundary treatment have been discussed. The performance of the modified WENO procedure has been examined and evaluated throughout a few applications in some typical aerodynamic flows including shock-boundary interactions and transonic flows around airfoils. It has been shown that the numerical accuracy and stability of the modified WENO procedure has been improved in comparison to that of the original WENO procedure by Shu ([9]). It has also been found that the modification made by Martin et al. ([11], [12]) in homogeneous turbulent flows is susceptible to numerical oscillations in general non-homogeneous cases. Preliminary application of this modified WENO scheme to high subsonic jet noise prediction has produced a very encouraging improvement over the low-order MUSCL Roe scheme. More studies and evaluations are needed before this modified WENO procedure could be fully applied to more complex aeroacoustic calculations. For example, the dispersion-preserving properties have to be evaluated as the modified WENO procedure adopts a fixed lower-order central scheme near the boundary points.

Acknowledgements

This work is supported by the US DOD SBIR Phase II contract N68335-07-C-0017, with Dr. John Spyropoulos as Technical Monitor.

References

[1] C.K.W. Tam, "Jet noise since 1952", Theo. Comput. Fluid Dynamics, Vol.10 (1998), p.393-405.

[2] C. Bogey and C. Bailly, "Computation of high-Reynolds number jet and its radiated noise using large eddy simulation based on explicit filtering," Computers and Fluids, 2006.

[3] C. Bogey and C. Bailly, "A family of low dispersive and low dissipative explicit schemes for flow and noise computations," J. of Computational Physics, Vol. 194(1), 2004, P.194-214.

[4] C. Bogey and C. Bailly, "Effects and inflow conditions and forcing on a Mach number 0.9 jet and its radiated noise," AIAA J. Vol.43(5), 2005, p.1000-1007

[5] D.J. Bodony and S. K. Lele, "On using large eddy simulation for the prediction of noise from cold and heated turbulent jets," Physics of fluids, Vol 17, 2005, p. 1-18.

[6] E.K. Koutsavdis, G.A. Blaisdell and A.S. Lyrintzis, "Compact schemes with spatial filtering in computational aeroacoustics," AIAA J. Vol.38(4), 2000, p.713-715.

[7] M.L. Shur, P.R. Spalart and M.Kh. Strelets, "Noise prediction for increasingly complex jets, Part I: Methods and Tests," International Journal of Aeroacoustics, Vol.4 (3+4), p.213-246, 2005.

[8] M.L. Shur, P.R. Spalart and M.Kh. Strelets, "Noise prediction for increasingly complex jets, Part II: Applications," International Journal of Aeroacoustics, Vol.4 (3+4), p.247-266, 2005.

[9] G.-S. Jiang, C.-W. Shu, Efficient implementation of weighted ENO scheme, J. of Computational Physics, 126 (1) (1996) 202-228.

[10] M.P. Martin, E.M. Taylor, M. Wu, V.G. Weirs, A bandwidth-optimized WENO scheme for the direct numerical simulation of compressible turbulence, J. of Computational Physics, 220 (1) (2006) 270-289.

[11] E.M. Taylor, M. Wu and M.P. Martin, Optimization of nonlinear error for WENO methods in direct numerical simulations of compressible turbulence, J. of Computational Physics, 223 (2007) 384-397.

[12] M.Visbal and D. Gaitonde, Shock capturing using compact-differencing-based methods, AIAA-Paper-2005-1265

[13] M.Visbal and D. Gaitonde, Very high-order spatially implicit schemes for computational acoustics on curvilinear meshes, J. of Computational Acoustics, 9 (4) (2001) 1259-1286.

[14] C.-W. Shu, Essentially non-oscillatory and weighted essentially non-oscillatory schemes for hyperbolic conservation laws, ICASE Report No. 97-65.

[15] A. Jameson, Analysis and Design of Numerical Schemes for Gas Dynamics 1 Artificial Diffusion, Upwind Biasing, Limiters and Their Effect on Accuracy and Multigrid Convergence, RIACS Technical Report 94.15, International Journal of Computational Fluid Dynamics, Vol. 4, 1995, pp. 171-218.

[16] J.L. Thomas and M.D. Salas, Far-field boundary conditions for transonic lifting solutions to the Euler equations, AIAA J. Vol.24 (7), p.1074-1080, 1986.

[17] A. Gross and H.F. Fasel, "High-order WENO schemes based on approximate Roe Riemann solver", AIAA-2002-2735.

[18] Y. Shen, B. Wang and G. Zha, "Implicit WENO scheme and high-order viscous formula for compressible flow", AIAA-2007-4431.

[19] M.Visbal and D. Gaitonde, "High-order-accurate methods for complex unsteady subsonic flows," AIAA J. Vol. 37(10), p.1231-1239,1999.

[20] H.K. Tanna, "An experimental study of jet noise, part II: shock associated noise." J. of sound and vibration (1977), 50(3):429-444.

[21] Cai, X., Ladeinde, F., Reba, R.A and Schlinker, R.H., "Hybrid LES/RANS calculation of high-speed jet noise,", AIAA-2007-3870.